Journal of Orthopaedic Translation 40 (2023) 1–12

Contents lists available at ScienceDirect

Journal of Orthopaedic Translation

journal homepage: www.journals.elsevier.com/journal-of-orthopaedic-translation

The effect of local sympatholysis on bone-tendon interface healing in a murine rotator cuff repair model

Tingmo Huang [a,b,c], Liyang Wan [a,b,c], Yang Chen [a,b,c], Yinghong Xiong [a,b,c], Feifei Yuan [b,c,d], Shanshan Xie [a,b,c], Jianjun Huang [e,**], Hongbin Lu [a,b,c,*]

[a] Department of Sports Medicine, Xiangya Hospital, Central South University, Changsha, 410008, China
[b] Key Laboratory of Organ Injury, Aging and Regenerative Medicine of Hunan Province, Changsha, 410008, China
[c] National Clinical Research Center for Geriatric Disorders, Xiangya Hospital, Central South University, Changsha, 410008, China
[d] Department of Spine Surgery and Orthopaedics, Xiangya Hospital, Central South University, Changsha, 410008, China
[e] Department of Orthopaedics, Ningde Affiliated Hospital, Fujian Medical University, Ningde, 352000, China

ARTICLE INFO

Keywords:
Bone-tendon interface healing
Sympathetic nerve
Norepinephrine
Adrenergic receptors

ABSTRACT

Background: Although neuroregulation plays an important role in tissue healing, the key neuroregulatory pathways and related neurotransmitters involved in bone-tendon interface (BTI) healing are still unknown. It is reported that sympathetic nerves can regulate cartilage and bone metabolism, which are the basic aspects of BTI repair after injury, through the release of norepinephrine (NE). Thus, the purpose of this study was to explore the effect of local sympatholysis (LS) on BTI healing in a murine rotator cuff repair model.

Methods: Specifically, C57BL/6 mice underwent unilateral supraspinatus tendon (SST) detachment and repair was established on a total of 174 mature C57BL/6 mice (12 weeks old): 54 mice were used to examine the sympathetic fibers and its neurotransmitter NE for the representation of sympathetic innervation of BTI, while the rest of them were randomly allocated into (LS) group and control group to verify the effect of sympathetic denervation during BTI healing. The LS group were intervened with fibrin sealant containing 10 ng/ml guanethidine, while the control group received fibrin sealant only. Mice were euthanized at postoperative 2, 4 and 8 weeks for immunofluorescent, qRT-PCR, ELISA, Micro-computed tomography (CT), histology and biomechanical evaluations.

Results: Immunofluorescence, qRT-PCR and ELISA evaluations indicated that there were the expression of tyrosine hydroxylase (TH), NE and β2-adrenergic receptor (β2-AR) at the BTI site. All the above showed a trend of increasing at the early postoperative stage and they started to decrease with the healing time after a significant peak. Meanwhile, local sympathetic denervation of BTI was achieved after the use of guanethidine as shown in the NE ELISA outcomes in two groups. QRT-PCR analysis revealed that the healing interface in the LS group expressed more transcription factors, such as *Runx2*, *Bmp2*, *Sox9*, and *Aggrecan*, than the control group. Further, radiographic data showed that the LS group significantly possessed higher bone volume fraction (BV/TV), trabecular number (Tb.N), trabecular thickness (Tb.Th), and lower trabecular spacing (Tb.Sp) than the control group. Also, histological test results showed that there was more fibrocartilage regenerated at the healing interface in the LS group compared with the control group. Mechanical testing results demonstrated that the failure load, ultimate strength and stiffness in the LS group were significantly higher at postoperative week 4 ($P < 0.05$), but not at postoperative week 8 ($P > 0.05$), compared to the control group.

Conclusion: The regulation of sympathetic innervation was involved in the healing process of injured BTI, and local sympathetic denervation by using guanethidine was beneficial for BTI healing outcomes.*The translational potential of this article*: This is the first study to evaluate the expression and specific role of sympathetic innervation during BTI healing. The findings of this study also imply that the antagonists of β2-AR could serve as a potential therapeutic strategy for BTI healing. Also, we firstly successfully constructed a local sympathetic denervation mouse model by using guanethidine loaded fibrin sealant, which provided a new effective methodology for future neuroskeletal biology study.

* Corresponding author. Xiangya Hospital, No. 87, Xiangya Road, Kaifu District, Changsha, 410008, China.
** Corresponding author. Ningde City Hospital, Fujian Medical University, Ningde, 352000, China.
E-mail addresses: fjhjj-a901@163.com (J. Huang), hongbinlu@hotmail.com (H. Lu).

https://doi.org/10.1016/j.jot.2023.03.001
Received 19 October 2022; Received in revised form 4 March 2023; Accepted 22 March 2023

1. Introduction

Bone-tendon interface (BTI) is an important part of the locomotor system, which is constituted by four continuous and functionally graded zones: tendon, unmineralized fibrocartilage, mineralized fibrocartilage and bone [1,2]. BTI connects soft tissue tendon/ligament and hard tissue bone, and its unique and complex gradient structure can effectively transfer mechanical load between tendon/ligament and bone, which is necessary for joint stability and mobility [2]. Injuries of BTI are common sports injuries in the field of orthopedics and sports medicine that leads to joint dysfunction and recurrent pain, which could occur in many parts of the body, such as rotator cuff, anterior cruciate ligament, Achilles tendon, etc. Take rotator cuff injury as an example, it is reported that more than 200,000 rotator cuff injuries require surgical reconstruction every year in the United States, and direct health treatment costs up to 474 million dollars [3]. In people over 50 years old with rotator cuff tear, the disability rate could reach as high as 30–50% [4]. How to promote BTI healing has been a challenge of clinicians.

BTI injuries occur between two different tissues, soft tissue tendon/ligament and hard tissue bone, with different mechanical properties and are mainly characterized by the damage of fibrocartilage. Due to poor blood supply and weak regeneration ability, BTI healing often results in poor recovery of biomechanical properties, disorder of matrix composition and structure, and fibrous scar healing [5,6]. Moreover, because that BTI is located at the site of stress concentration, palindromic raptures after repair are hard to prevent. For example, although the surgical techniques for rotator cuff tear have progressed during the past decades, unfortunately, the postoperative retear rate observed was still up to 20%–90% [7]. Previous studies suggested that the regeneration of fibrocartilage is closely related to the healing quality of BTI, promoting the expression of chondrogenic transcription factors Runx2 etc. can facilitate BTI healing [8,9]. Therefore, promoting the regeneration of fibrocartilage layer is the key to realize the rapid and high-quality healing of BTI.

In recent years, more and more studies have suggested that the role of nervous system in the healing process of musculoskeletal system cannot be ignored. Neuroregulation is involved in growth, development and function maintenance of the fibrocartilage, lacking of which will lead to disorganized chondrogenesis and deformed fibrocartilage layer [10]. Although there is few studies and literature about the function of neuroregulation in BTI healing, neurostimulation techniques represented by functional electrical stimulation, combined magnetic field and other biophysical therapies have been confirmed could effectively promote the regeneration of fibrocartilage and accelerate the recovery of motor function in patients with injuries of BTI [5,11]. It has been proven that CGRP, SP and NPY are an important component of BTI healing microenvironment and participate in the healing process of BTI [12,13]. These studies suggested that neuromodulation plays a crucial part in enthesis regeneration. However, it is still necessary to further explore the key neural regulatory pathways and related neurotransmitters involved in BTI healing.

There are mainly autonomic, sensory and glutamic-energic neural pathways involved in the healing process of musculoskeletal system, among which the autonomic nervous system is considered critical for maintaining regional homeostasis and regulating local metabolism [14,15]. However, the relation between sympathetic nervous system and BTI healing has not been investigated yet. Studies have shown that sympathetic nerve fibers participate in a variety of physiological and pathological processes, such as inflammation regulation [15], chondrocyte and osteocyte metabolism [16,17], differentiation of mesenchymal stem cells [18], etc., through the release of norepinephrine (NE). While these processes are related to the BTI healing, we thus speculate that sympathetic nerve fibers may also exert their effects during BTI healing. Therefore, the purposes of the current study were to detect the sympathetic innervation of BTI after injury and to verify the role it plays in BTI healing by blocking NE release through the topical administration of guanethidine, a neurotoxin which specifically target sympathetic nerve fibers to block the release and reuptake of NE.

2. Materials and methods

All animal care and experimental procedures were approved by the laboratory animal committee of Xiangya Hospital of Central South University (No. 2022020210).

2.1. Study design

A total of 174 male C57BL/6 mice (12 weeks old) were used for the rotator cuff repair model, which was established on the left shoulder, according to a previously reported method [19]. 54 mice were used to examine the expression of tyrosine hydroxylase (TH), a marker of sympathetic fibers, and neurotransmitter NE for the representation of sympathetic innervation in the BTI healing site, then the rest were randomly assigned to either the control group or the LS group with 60 mice in each group. Mice in the LS group were intervened with fibrin sealant containing 10 ng/ml guanethidine, which has functional sympathectomy effect through the blockade of neural transmission, depletion of neuronal NE stores, and blockade of reuptake of NE into the neurons [20], while the control group received fibrin sealant only. Mice were euthanized postoperatively to harvest bilateral supraspinatus tendon-humerus (SSTH) complex for subsequent tests. In order to detect the sympathetic innervation at the healing site, specimens were used for immunofluorescence staining, quantitative reverse-transcription polymerase chain reaction (qRT-PCR) and NE ELISA at postoperative 2, 4 and 8 weeks (Fig. 1A). Then, to evaluate the quality of the healing site after blocking the release of NE, specimens from two groups were used for qRT-PCR, Micro-computed tomography (Micro-CT), histological evaluations and biomechanical tests (Fig. 1B).

2.2. Preparation of fibrin sealant carrier

To fabricate the fibrin sealant, fibrinogen solution (Sigma–Aldrich) and thrombin solution (Sigma–Aldrich) were prepared according to the manufacturer's manual. Guanethidine was added to the thrombin solution. The fibrin sealant was fabricated following a method reported previously [21]. Then, two groups were formed: control group with fibrin sealant alone and LS group with fibrin sealant containing 10 ng/ml guanethidine.

2.3. Animal model and LS treatment

All mice underwent unilateral supraspinatus tendon (SST) detachment and repair in the left shoulder after anesthetized with an intraperitoneal injection of 0.3% pentobarbital sodium (0.6 mL/20 g; Sigma–Aldrich) following a previously reported protocol [22]. All procedures were performed under sterile technique using a surgical microscope. In brief, a longitudinal skin incision was made on the left shoulder after mice were placed in a right lateral decubitus position. Then, the deltoid muscle was revealed, which was split with a transverse cut to expose the SST. Using a customized retractor to pull away the acromion to improve visualization. The SST was then fixed with No. 6–0 PDS suture (Ethicon, Somerville, NJ) in an "8" figure pattern, the SST was transected at its insertion site on the humeral head, and the cartilage layer at the insertion site was gently removed with a scalpel to expose the bellowing spongy bone. One 1-mm diameter transosseous tunnel was created transversely within the humeral head, and the PDS suture was crossed through the bone tunnel. At this point, 10 μL fibrin sealant was placed between the SST and bone, the animals were assigned to two groups: Control group (fibrin sealant alone), LS group (fibrin sealant containing 10 ng/ml guanethidine). Then, the SST was tied to its original insertion site after tightening the two sutured limbs. Finally, the deltoid and skin were sutured. All mice were allowed free cage activity after surgery.

Antibiotic injections (penicillin G) were administrated once a day for 3 days after surgery.

2.4. Immunofluorescence analysis

Immunofluorescence was used to detect the expression of TH, a marker of sympathetic nerve fibers, and β2-adrenergic receptor (β2-AR) in the BTI healing site. Briefly, the supraspinatus tendon-humerus (SSTH) specimens were harvested at postoperative weeks 2, 4 and 8, then fixed with 4% paraformaldehyde (PFA) for 24 h. After decalcification, dehydration and embedded in OCT, the SSTH specimens were longitudinally sectioned with 10 μm thickness. For immunofluorescent staining, the sectioned slices were washed with PBS and then blocked with 5% bovine serum albumin (BSA) for 1 h. Then, primary antibodies anti-TH (AB152; Millipore) and anti-β2-AR (DF3512; Affinity) were applied respectively at 4 °C overnight, the sections were incubated with secondary antibodies anti-rabbit Alexa Fluor 488 (ab150073; Abcam) or Alexa Fluor 594 (ab150064; Abcam) for 1 h subsequently. Finally, the slices were counterstained with 4', 6-diamidino-2-phenylindole (Invitrogen, Carlsbad) to observe the tissue morphology and distinguish the BTI site. All images were observed and captured using a Zeiss Axio Imager. M2 microscope (Zeiss, Solms, Germany) equipped with an Apotome. 2 System. To analyze the positive signals of TH and β2-AR, a region of interest (ROI) was defined at the BTI site according to a similar study reported previously [23]. At last, using the Image J software to measure the integrated optical density (OD) of positive areas. The assessors were blinded to the groups during image analysis.

2.5. Gene expression analysis

The mRNA expression levels of relevant factors (*TH*, *ARs*, *Runx2*, *Bmp2*, *Sox9* and *Aggrecan*) at the BTI healing site were measured by real-time quantitative reverse transcription polymerase chain reaction (qRT-PCR). The regenerated BTI tissues for qRT-PCR analysis were collected using a microscope according to a previous protocol [19]. Briefly, after the SSTH specimens were harvested and frozen in liquid nitrogen, we removed the muscle belly and kept the tendon (one millimeter in length) and the portion of the humeral head proximal to the growth plate near the tendon attachment. The weight of each sample was adjusted to be around 20 mg. Total RNA was extracted from the tissue using the TRIzol reagent (Invitrogen), and cDNA was synthesized using 1 mg of total RNA with a GoScript™ Reverse Transcription System (Promega) following the manufacturer's instructions. Then, the qRT-PCR reactions were performed on ABI PRISM® 7900HT System (Applied Biosystems) with GoTaq® qPCR Master Mix (Promega). Glyceraldehyde 3-phosphate dehydrogenase (GAPDH) was used as a reference gene for normalization and the $2^{-\Delta\Delta Ct}$ method was used to analyze the relative expression. The primers used for the qRT-PCR assay in the current study are provided in Table 1.

2.6. Enzyme-linked immunosorbent assay (ELISA)

To evaluate the levels of NE in the BTI healing site, the regenerated BTI tissues were harvested at postoperative weeks 2, 4 and 8 respectively. Using ELISA methods to detect the expression of NE in the enthesis according to the instructions of the NE ELISA kit (E-EL-0047c; Elabscience Biotechnology). Then, the absorbance was measured at 450 nm using an enzyme-labelled meter (Multiskan Mk3; Thermo Fisher Scientific). Each sample was repeated in triplicate and measure the average value.

2.7. Radiological analysis

Micro-CT (viva CT 80; Scanco Medical, Brüttisellen, Switzerland) was performed in this study to evaluate the formation of subchondral bone at the SST attachment site. After SSTH specimens were harvested from each group, the samples were fixed in 4% PFA at 4 °C for 24 h and then washed with 0.9% saline to remove the residual PFA. After that, the samples were placed in a tube with their long axes in the vertical position and scanned with Micro-CT following these conditions: 10.4 μm voxel size, 55 KVp, 0.36° rotation step (180° angular range), and a 400 ms exposure per view. Scanning data of each specimen were processed with a 3-dimensional Gaussian filter and a global threshold to distinguish the bone voxels from the surrounding soft tissues and bone marrow. The region of interest (ROI) was selected under the footprint at the center of the 2 suture bone holes in the image according to a previously reported method [24]. Then, morphological parameters of the newly formed bone including bone volume fraction (BV/TV), trabecular number (Tb.N), trabecular thickness (Tb.Th), and trabecular spacing (Tb.Sp) were measured.

2.8. Histological analysis

After micro-CT analysis, the SSTH specimens were decalcified with 10% ethylenediaminetetraacetic acid (EDTA) at room temperature for 14 days. After dehydrated in grade ethanol and embedded in paraffin, the specimens were cut into 6 μm–thick sections in the coronal plane through the greater tuberosity and SST by use of a microtome (Leica RM2125; Reichert-Jung GmbH). Then, the sections were stained with hematoxylin and eosin (H&E) or toluidine blue & fast green (TB&FG) (Sigma–Aldrich) after deparaffinized and rehydrated. Using light microscopy (CX31, Olympus, Germany) to observe histologic sections under the same condition. The H&E stained sections were used for the histological description of BTI healing and semi-quantitative analysis for fibrocartilage area. Toluidine blue/fast green stained sections were used for semi-quantitative analysis of the integrated optical density (IOD) of proteoglycan using the ImageJ software (National Institutes of Health,

Table 1
The primers used for qRT-PCR.

Gene Name	NCBI Reference	Forward (5′-3′)	Reverse (5′-3′)
GAPDH	NM_008084	AACGACCCCTTCATTGACCTC	ACTGTGCCGTTGAATTTGCC
TH	NM_009377	GTCTCAGAGCAGGATACCAAGC	CTCTCCTCGAATACCACAGCC
ADRA1A	NM_013461	CTAAGGCCATTCTACTTGGGGT	CGAGTGCAGATGCCGATGA
ADRA1B	NM_007416	GCAGCGGTTGATGTCCTGT	AGTATCGCACCCCAATGTAGC
ADRA1D	NM_013460	AGTGGGTGTCTTCCTAGCC	GCCTAGAACCTCCATAGTGGC
ADRA2A	NM_007417	GGTGACACTGACGCTGGTTT	ACTGGTGAACACCGCGATAATA
ADRA2B	NM_009633	TCTTCACCATTTTCGGCAATGC	AGAGTAGCCACTAGGATGTCG
ADRA2C	NM_007418	CTGTGGTGGGTTTCCTCATCG	ACTTGCCCGAAGTACCAGTAG
ADRB1	NM_007419	CTCATCGTGGTGGGTAACGTG	ACACACAGCACATCTACCGAA
ADRB2	NM_007420	GGGAACGACAGCGACTTCTT	GCCAGGACGATAACCGACAT
ADRB3	NM_013462	GGCCCTCTCTAGTTCCCAG	TAGCCATCAAACCTGTTGAGC
Runx2	NM_001146038	GACTGTGGTTACCGTCATGGC	ACTTGGTTTTTCATAACAGCGGA
Sox9	NM_011448	AGTACCCGCATCTGCACAAC	ACGAAGGGTCTCTTCTCGCT
Aggrecan	NM_007424	GTGGAGCCGTGTTTCCAAG	AGATGCTGTTGACTCGAACCT
Bmp2	NM_007553	GGGACCCGCTGTCTTCTAGT	TCAACTCAAATTCGCTGAGGAC

Bethesda, MD, USA) [25]. The histological images were semi-quantitatively analyzed by two blinded observers.

2.9. Biomechanical testing

Biomechanical testing is an important indicator of the quality of BTI healing. The failure load, ultimate strength and stiffness of the SSTH specimens were detected with a biomechanical testing system (model 5942; Instron) according to a previously reported method [26]. Before the test, all the samples were thawed for 4 h at 4 °C and then 1 h at room temperature. The width and thickness of the enthesis were measured with a caliper under the same tensile load (0.1 N) and then the cross--sectional area was calculated. After that, the humerus was firmly clamped with a vise grip, while the SST was fixed in a clamp with sandpaper. The SSTH specimens was placed into the testing system machine for uniaxial tension following the SST's approximate anatomic position. The samples were preconditioned with a load of 0.1 N and then loaded to failure at a rate of 0.03 mm/s, and the ultimate failure load and distance at max load were recorded. The stiffness was calculated from the curve of the load to deformation. Data were excluded if the tendon slipped out of the grip or did not fail at the SST attachment site.

2.10. Statistical analysis

All statistical analyses were performed using SPSS 25.0 software (SPSS Inc). All quantitative data were presented as mean ± SD (standard deviation) and were analyzed statistically using a 2-way analysis of variance (ANOVA) with the Bonferroni post hoc test to detect differences between two groups. Statistical significance was set at $P < 0.05$.

3. Results

3.1. Distribution of TH-positive nerve fibers in BTI healing site

A peak in TH immunoreactivity was observed at postoperative week 4 in the SST zone surrounding the enthesis, whereas few nerve fibers were found on the native enthesis. These nerve fibers were seen as new sympathetic nerve fibers sprouting into the SST from the surrounding structures. At postoperative week 8, during the enthesis healing, most of the TH-positive fibers retracted from the healing site (Fig. 2A). Furthermore, there was a statistically significant increase in the mRNA expression levels of TH at the healing site at postoperative weeks 2, 4 and 8 as compared to native enthesis ($P < 0.05$ for all) (Fig. 2B).

3.2. AR profile in BTI healing site

The normal BTI expressed mRNA for various subtypes of α- and β-AR, which also expressed in the BTI sites of SSTH specimens with different postoperative times. A high level of β2-AR mRNA was detected in BTI healing site, while a weak expression of β3-AR was observed (Fig. 3A). Protein expression and localization of β2-AR were determined in cryostat sections of SSTH samples. Immunofluorescence for β2-AR revealed a positive signal in the fibrocartilage zone (Fig. 3B). There were significant increases of the number of $\beta2\text{-AR}^{+}$ cells/HPF (high power field) at postoperative weeks 2 and 4 compared with native enthesis and 8 weeks of healing (Fig. 3D), which consistent with the mRNA expression level of β2-AR in the BTI healing site (Fig. 3C). At postoperative week 4, the expression of β2-AR was at peak, then decreased along with the healing time.

3.3. NE levels in serum and BTI healing site

NE levels of BTI healing site, but not serum NE levels, significantly changed at different times after surgery. NE levels of BTI healing site at postoperative weeks 2 and 4 were significantly higher than native enthesis and 8 weeks of healing ($P < 0.05$) (Fig. 4A), while serum NE levels at different times after surgery were not significantly different from each other ($P > 0.05$) (Fig. 4B).

In mice subjected to guanethidine treatment, the decrease of NE content in BTI healing site observed after operation was indicative of the success of local sympathetic denervation. Significantly decreased NE levels of BTI healing site observed in the LS group at postoperative weeks 2 and 4 when compared to the control group ($P < 0.05$) (Fig. 4C).

3.4. The expression of growth factors in enthesis

The qRT-PCR results (Fig. 5) showed that the mRNA expression level of transcription factors (*Runx2*, *Bmp2*, *Sox9*, and *Aggrecan*) was higher in the LS group as compared to those in the control group. Among the transcription factors, the expression of runx2 was significantly higher at postoperative week 4 in the LS group than in the control group ($P < 0.001$), but there were no significant differences between them at weeks 2 and 8 ($P > 0.05$ for both). At postoperative week 2, the expression of sox9 and aggrecan were at peak, then decreased along with the healing

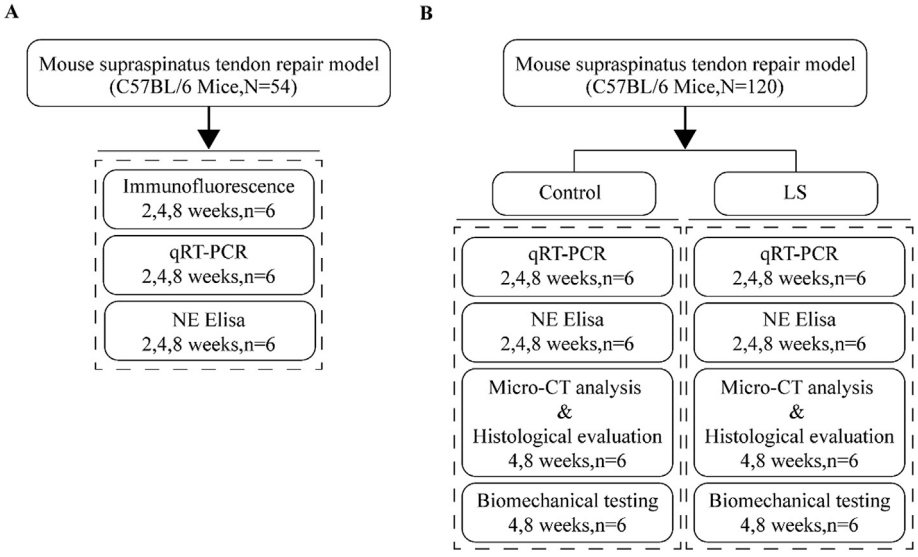

Figure 1. Study design (A) To detect the sympathetic innervation in BTI healing site (B) To verify the role of sympathetic innervation during BTI healing. qRT-PCR: quantitative reverse-transcription polymerase chain reaction. LS: local sympatholysis.

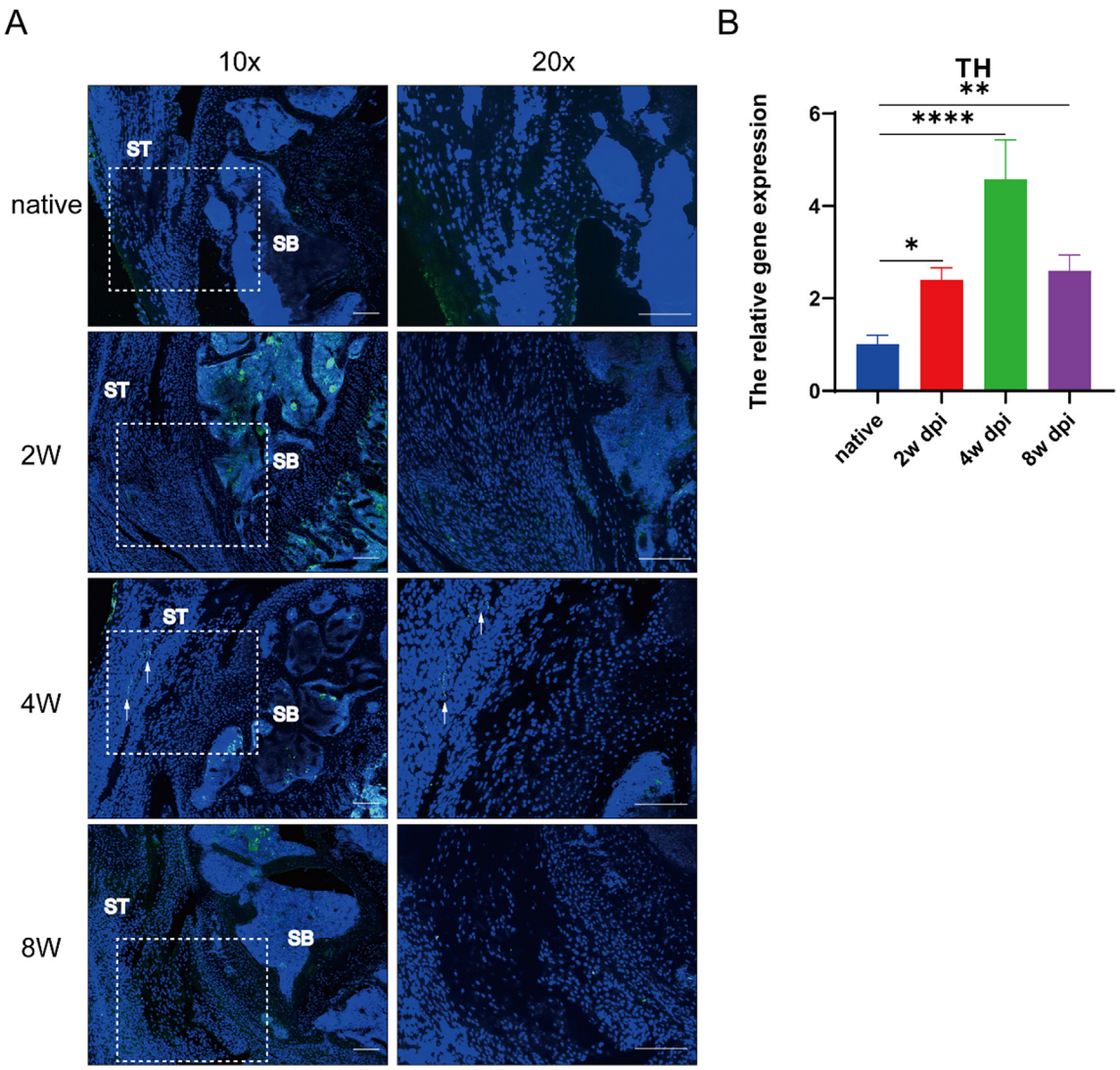

Figure 2. (A) Immunofluorescence staining of TH at different times during BTI healing. The regions marked by dashed line in the 10x pictures are amplified in corresponding 20x pictures. Scale bars indicate 100 μm. The white arrow marks the new sprouting sympathetic nerve fibers (B) The mRNA expression levels of TH at different times during BTI healing. dpi: days post injury. SB: subchondral bone; ST: supraspinatus tendon; *P < 0.05, **P < 0.01, ***P < 0.005, ****P < 0.001.

time in both groups. Sox9 and aggrecan levels were significantly higher in the LS group than the control group at week 2 postoperatively (P < 0.001 for both), while the expression of bmp2 in the LS group was higher than that in the control group at weeks 2, 4 and 8 postoperatively (P < 0.001 for all).

3.5. Microstructural analysis

After micro-CT scanning, the three-dimensional morphologic of the SSTH was constructed, and the microstructural parameters of the subchondral bone at the BTI healing site were analyzed (Fig. 6). From the 3D visualization images of the SSTH, increases of subchondral bone formation at the enthesis healing site were observed with healing time increasing from both groups (Fig. 6A). There was more bone mass at the BTI site in the LS group as compared to the control group at postoperative weeks 4 and 8 from the surface pictures. The microstructure data showed that the healing interface of the LS group was shaped better than that of the control group at postoperative weeks 4 and 8. The LS group had significantly greater BV/TV (0.345 ± 0.009), Tb.N (19.700 ± 0.812 mm^{-1}), and Tb.Th (0.021 ± 0.0004 mm) at postoperative week 4 than the control group (BV/TV: 0.304 ± 0.016, P < 0.001; Tb.N: 17.060 ± 0.463 mm^{-1}, P < 0.001; Tb.Th: 0.019 ± 0.0005 mm, P < 0.001), while the Tb.Sp in the LS group (0.336 ± 0.011 mm) were lower than that in the control group (0.392 ± 0.011 mm, P < 0.001). At postoperative week 8, the bone morphological parameters including BV/TV, Tb.N, Tb.Th and Tb.Sp were improved during enthesis healing in both groups. Also, the BV/TV (0.507 ± 0.013), Tb.N (24.760 ± 0.531 mm^{-1}), and Tb.Th (0.025 ± 0.0005 mm) of the LS group were significantly higher than those of the control group (BV/TV: 0.464 ± 0.010, P < 0.001; Tb.N: 22.110 ± 0.529 mm^{-1}, P < 0.001; Tb.Th: 0.026 ± 0.0006 mm, P > 0.05), while the Tb.Sp in the LS group (0.258 ± 0.012 mm) were lower than that in the control group (0.286 ± 0.009 mm, P < 0.01) at week 8 postoperatively (Fig. 6B).

3.6. Histological assessments

The representative images of H&E staining and TB&FG staining showed a more mature tendon-to-bone attachment in the LS group compared with the control group at postoperative weeks 4 and 8. The H&E staining (Fig. 7A) showed that the regenerated interfaces were visible between the SST and humerus at weeks 4 and 8 after surgery. It also showed that the enthesis was gradually regenerated with time. At postoperative week 4, tissue connecting tendon and bone was poorly organized and highly cellular in two groups. The TB&FG staining (Fig. 7B) showed some TB deposited at the attachment site, especially at

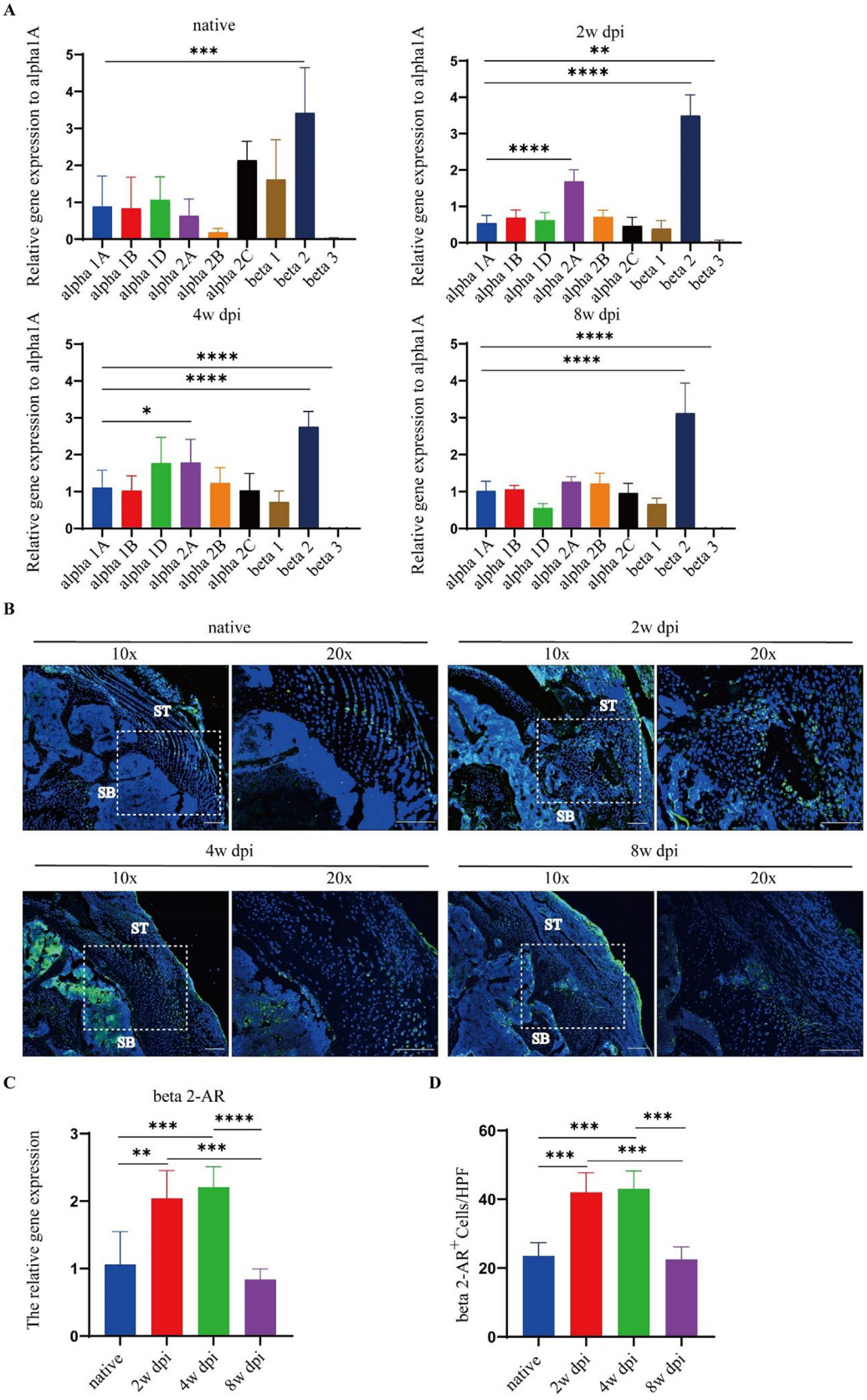

Figure 3. Expression of AR subtypes in BTI healing site (A) The relative gene expression of AR subtypes was analyzed in the BTI healing site. Gapdh expression was used as a loading control (B) Protein expression and localization of β2-AR in enthesis were analyzed on cryo-sections (C) The mRNA expression level of β2-AR in the BTI healing site at different time points after surgery (D) The change of the number of ADRB2^{+} cells/HPF during BTI healing. The regions marked by dashed line indicate the position of BTI. dpi: days post injury. Scale bars indicate 100 μm *P < 0.05, **P < 0.01, ***P < 0.005, ****P < 0.001.

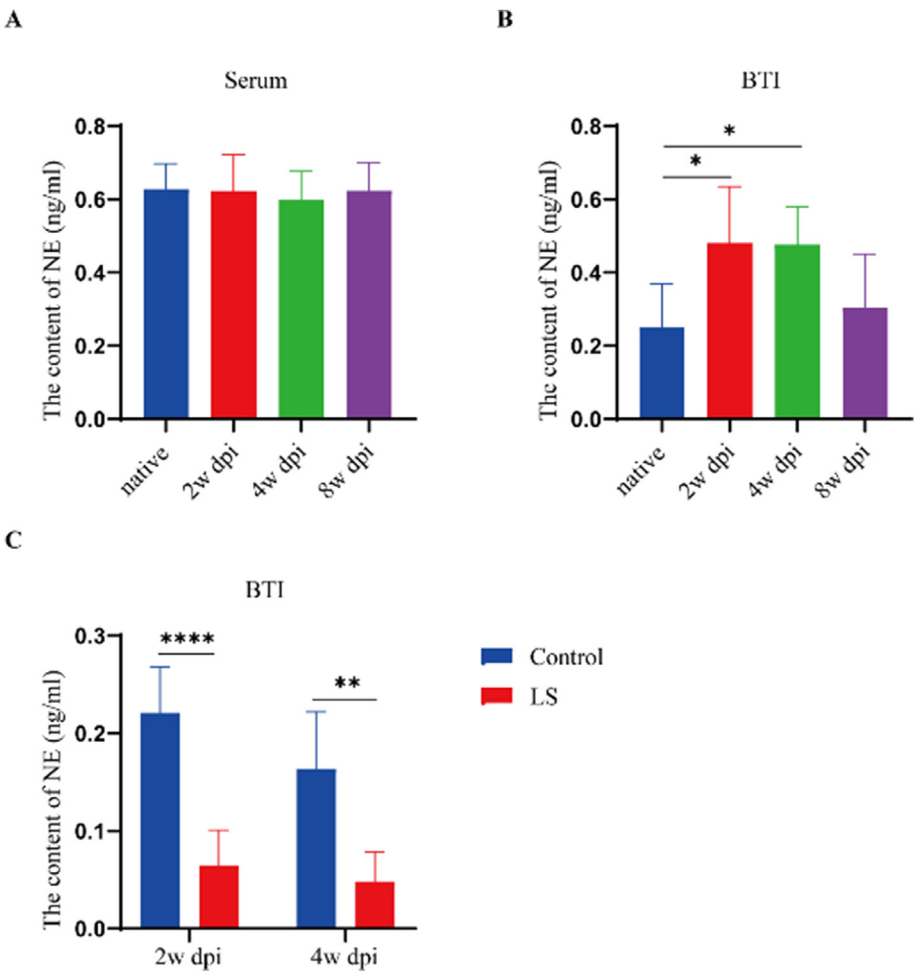

Figure 4. NE levels in serum (A) and BTI healing site (B–C) during enthesis healing examined. dpi: days post injury. *P < 0.05, **P < 0.01, ***P < 0.005, ****P < 0.001.

week 8 after surgery, which indicated the formation of fibrocartilage. Quantitively, there were no significant differences in the area of the regenerated fibrocartilage zone between two groups at postoperative weeks 4 and 8 ($P > 0.05$ for both) (Fig. 7C). The integrated optical density (IOD) of proteoglycan deposition at the BTI healing site in the LS group was significantly higher than the control group at 4 and 8 weeks after surgery ($P < 0.05$ for both) (Fig. 7D).

3.7. Biomechanical evaluation

The biomechanical testing results showed that healing of the BTI was enhanced with time. The diagram of biomechanical testing are shown in Fig. 8A. Although there were no significant difference in general appearance between two groups (Fig. 8B), at postoperative week 4, the LS group had a significantly higher failure load, ultimate strength and stiffness as compared to those in the control group (failure load, 4.38 ± 0.37 vs 3.72 ± 0.52 N, $P < 0.05$; ultimate strength, 3.79 ± 0.21 vs 3.13 ± 0.33 MPa, $P < 0.01$; stiffness, 3.68 ± 0.17 vs 3.32 ± 0.24 N/mm, $P < 0.05$), while the differences between them in two groups narrowed at week 8 postoperatively (failure load, 5.27 ± 1.11 vs 5.02 ± 0.37 N; ultimate strength, 5.26 ± 0.96 vs 5.10 ± 0.19 MPa; stiffness, 3.74 ± 0.40 vs 3.43 ± 0.28 N/mm, $P > 0.05$ for all). In addition, no significant difference was seen in cross-sectional area between the LS group and the control group at postoperative week 4 (1.15 ± 0.04 mm^2 vs 1.19 ± 0.05 mm^2, $P > 0.05$) and week 8 (1.00 ± 0.03 mm^2 vs 0.98 ± 0.04 mm^2, $P > 0.05$) (Fig. 8C).

4. Discussion

This study demonstrated the involvement of the sympathetic innervation in BTI healing. QRT-PCR, immunofluorescence and ELISA results showed that there were the expression of TH, NE and related adrenergic receptors (ARs) at the healing site. We also found that there were sympathetic nerve fibers sprouting into the SST during the healing process, which emerged at the early stage of healing and returned to the level of normal as time went on. Studies have shown that innervation of intact healthy tendons mainly existed in the surrounding structures, such as paratenon, endotenon and epitenon, whereas the innervation of tendon proper was scarce. However, it is found that extensive nerve fibers could ingrowth into the tendon proper after injury and during repair, then different neuronal mediators began to emerge to regulate the tendon regeneration. After the healing process finished, the newly grown nerve fibers within the tendon proper would retract [27,28]. The process of nerve fibers regeneration during BTI healing is consistent with the observations on bone [29], ligament [30] and skin [31] healing indicating that nerve ingrowth and subsequent retraction are fundamental aspects of tissue repair.

Nerve fibers can exert regulatory effect on target tissues through the release of neurotransmitters. Evidences of neurotransmitters involved in tissues regeneration after injury have been reported previously [32,33]. Also, neurotransmitters are important components of BTI healing microenvironment and involved in the healing process of enthesis [12]. The sensory neuropeptides (CGRP and SP) and sympathetic neuropeptide NPY were found in the enthesis, and the expression pattern of them were

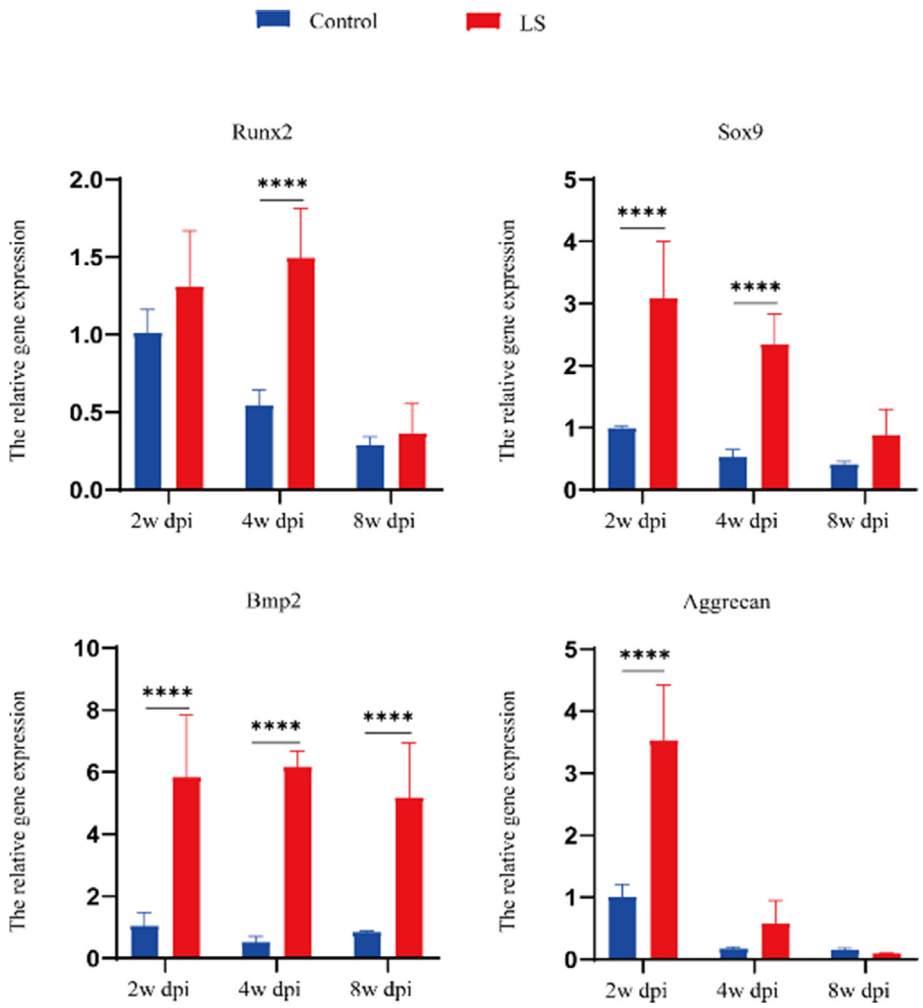

Figure 5. The quantitative reverse transcription polymerase chain reaction analysis of Runx2, Bmp2, Sox9, and Aggrecan expression in BTI healing site in two groups at postoperative weeks 2, 4 and 8. dpi: days post injury. *P < 0.05, **P < 0.01, ***P < 0.005, ****P < 0.001.

similar, all increased at the early stage of healing then decreased till the end of the healing process [12,13]. Our results showed that NE, the major neurotransmitter of sympathetic nerve fibers, was participated in BTI healing. Moreover, the content of NE at the healing site presented the same regularity as the other neuropeptides above.

Most neurotransmitters work by binding to related receptors. ARs mediate the effects of NE, the major sympathetic neurotransmitter, and play an important role in various physiologic and pathologic processes [34,35]. Nine AR subtypes have been identified and categorized into three subfamilies. The α1-AR subfamily includes the subtypes α1a, α1b, and α1d; the α2-AR subfamily includes the subtypes α2a, α2b, and α2c; and the β-AR subfamily includes the subtypes β1, β2, and β3 [36]. J Lorenz et al. [17] detected different AR subtypes in chondrocytes indicating that chondrocytes could response to the stimulation of the sympathetic nervous system. In the skeletal system, as is reported, β2-AR is the major mediator of catecholamine activation in bone remodeling units [37]. However, which ARs are expressed at the BTI has not been investigated so far. In the current study, we found that there were gene expression of various ARs, especially β2-AR, in BTI healing site according to the qRT-PCR results. Immunofluorescent staining further showed that $\beta2\text{-AR}^{+}$ cells existed in BTI site and the expression pattern of β2-AR was similar to the TH and NE. Thus, we speculated that the sprouting sympathetic nerve fibers in the SST surrounding enthesis might act on β2-AR, by releasing NE and spreading to the healing site, to regulate the BTI healing.

To investigate the role of the sympathetic innervation plays during BTI healing. Guanethidine was utilized in this study to create local chemical sympathectomy of rotator cuff. According to the NE ELISA results, the content of NE at the healing site subjected to the chemical sympathectomy treatment was lower than the control group, indicating that local functional sympathetic nervous system denervation of BTI was achieved through the use of guanethidine. In recent years, a growing body of research has shown that sympathetic upregulation exerts an adverse effect on cartilage and bone regeneration [38–41], while promoting the regeneration of cartilage and bone is beneficial to BTI healing [8,9]. It has been reported that NE treatment dose-dependently inhibits chondrogenic differentiation of mesenchymal stem cells (MSCs), while the use of nadolol, a β2-AR antagonist, could reverse this inhibition impact [38]. Hedderich J et al. [39] verified that the inhibition effect of NE on MSCs was realized via β2-AR mediated ERK1/2 and PKA phosphorylation. NE released by sympathetic nerve fibers could stimulate the β2-AR of osteoblasts and osteocytes, which leads to inhibited of bone formation and promoted bone resorption, inducing bone loss [41]. K Jiao et al. [42] found that NE caused condylar subchondral bone loss under stress of chronic immobilization, which could be prevented by chemical sympathectomy treatment. Hence, the sympathetic innervation might exert a negative effect on BTI healing and our results confirmed this viewpoint.

We firstly established a local sympathetic denervation mouse model by using guanethidine loaded fibrin sealant, which have been proved reliable, effective and repeatable through repetitive quantitative ELISA tests. We believe that this is a methodology worth further researching

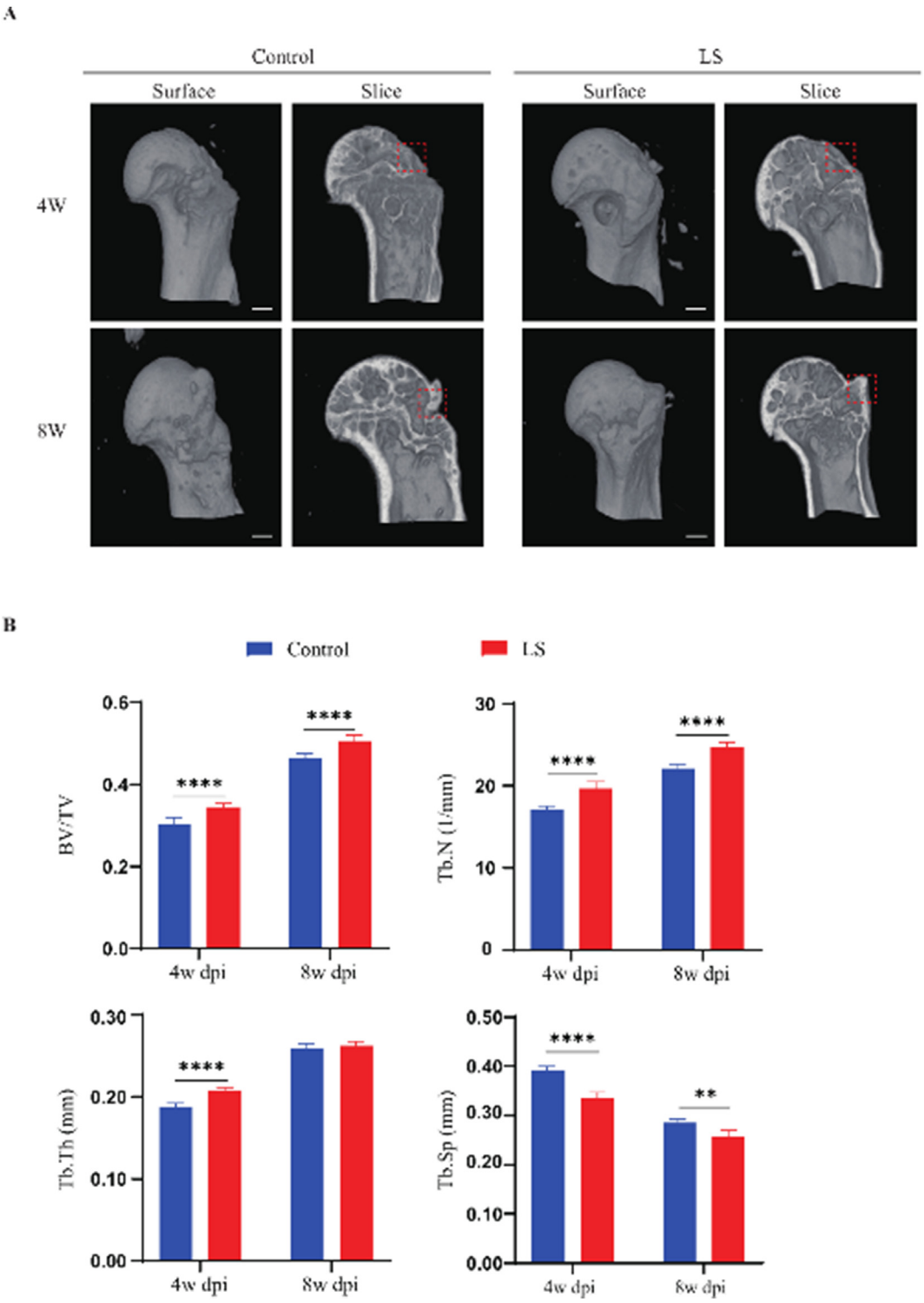

Figure 6. (A) Three-dimensional reconstruction images and sagittal sections of SST enthesis from LS and control groups at postoperative weeks 4 and 8. The red dotted box is the selected area of the region of interest for further statistical analysis of the bone morphological parameters. Scale bar indicates 500 μm (B) The morphological parameters of subchondral bone in each group at postoperative weeks 4 and 8. BV/TV, bone volume/total volume fraction; Tb.N, trabecular number; Tb.Th, trabecular thickness; Tb.Sp, trabecular separation; dpi: days post injury. *P < 0.05, **P < 0.01, ***P < 0.005, ****P < 0.001. (For interpretation of the references to colour in this figure legend, the reader is referred to the Web version of this article.)

and extending. This study showed that the local sympathetic denervation treatment might facilitate the enthesis healing, as evidenced by the improved BV/TV, Tb.N, Tb.Th and the reduced Tb.Sp as compared to the control group according to the micro-CT results. QRT-PCR results also indicated that more osteogenic and chondrogenic transcription factors were formed at the healing site in the LS group when compared to the control group. Meanwhile, there were better maturity and more proteoglycan, a component of the extracellular matrix of cartilage, at the enthesis after local sympathetic denervation treatment shown in H&E staining images and toluidine blue/fast green staining images

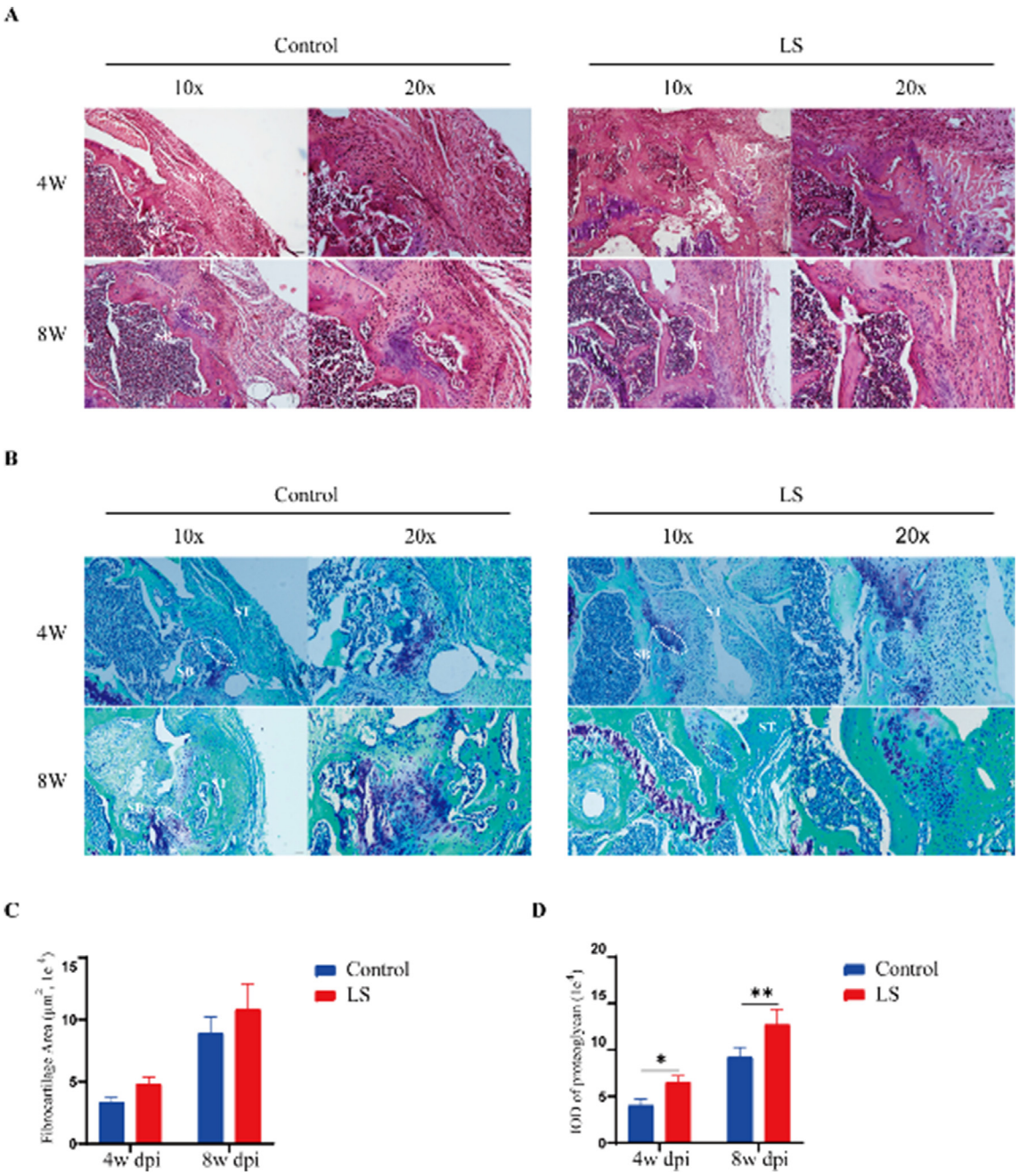

Figure 7. (A) Representative H&E images of BTI healing site at postoperative weeks 4 and 8 (B) Representative Toluidine blue/fast green images of BTI healing site at postoperative weeks 4 and 8. Comparison of (C) the area of regenerated fibrocartilage-like tissue and (D) integrated optical density (IOD) of the proteoglycan between the two groups at different time points. The regions marked by dashed line in the 10x pictures are amplified in corresponding 20x pictures. Scale bars indicate 200 μm for 10x and 100 μm for 20x. SB: subchondral bone; ST: supraspinatus tendon; dpi: days post injury. *P < 0.05, **P < 0.01. (For interpretation of the references to colour in this figure legend, the reader is referred to the Web version of this article.)

respectively. The better healing of BTI in the LS group might account for the improvement in biomechanical properties as shown by higher failure, ultimate strength and stiffness at postoperative week 4 in biomechanical testing. At postoperative week 8, however, the differences of biomechanical properties between two groups narrowed. Therefore, these analyses demonstrated that the sympathetic innervation might have a negative impact on BTI healing and blocking the release of NE through local sympathetic denervation treatment could accelerate the enthesis healing.

It is reported that estrogen is involved in subchondral bone and cartilage matrix remodeling, which are the basic aspects of BTI healing. Thus, we chose the male mice as the research object to avoid the effects of estrogen on BTI healing [43]. There were some limitations in the present study. First, the mouse model used for acute SST injury repair might not be fully applicable to humans for the differences in anatomy and healing capacity between mice and humans. Second, no reliable immobilization of the injured shoulder was performed in our study, an additional immobilization group would reinforce the experiment design. Finally, although we found that the sympathetic innervation was involved in the healing process of BTI, the molecular mechanisms by which the sympathetic innervation regulated the enthesis healing required further exploration.

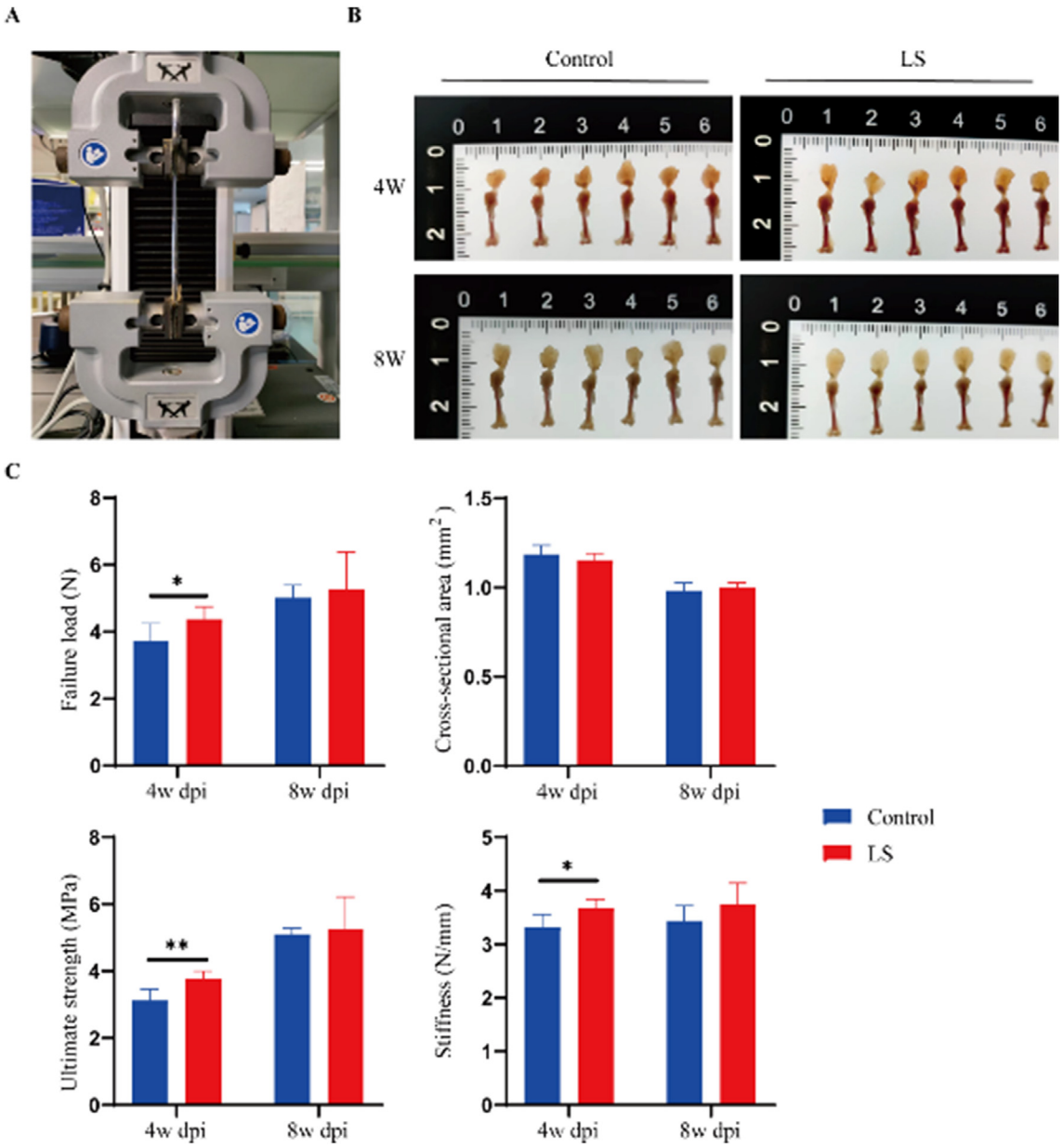

Figure 8. (A) The diagram of the biomechanical testing (B) The appearance of the SSTH complex at postoperative weeks 4 and 8 in two groups (C) The biomechanical properties of the SSTH complex. dpi: days post injury. *P < 0.05, **P < 0.01.

5. Conclusion

In conclusion, the sympathetic innervation is involved in BTI healing, which may play an inhibitory role by releasing NE. Through the use of guanethidine, a sympathetic nerve agent, to inhibit the release of NE seems to improve the healing quality of BTI. However, the underlying mechanism of how the sympathetic innervation acts on the enthesis healing needs to be further studied. The current study may provide a new therapeutic method for the clinical treatment on BTI injuries. Also, we firstly successfully constructed a local sympathetic denervation mouse model by using guanethidine loaded fibrin sealant, which worth further study and extending.

Author contributions

TH and LW: performed experiments, wrote the manuscript. **YC**: analyzed data. **YX, FY and SX**: assisted in the experiments and preparation of the manuscript. **HL and JH**: designed experiments, project administration. All authors read and approved the final manuscript. **TH and LW** contributed equally to this work.

Declaration of competing interest

The authors declare that they have no known competing financial interests or personal relationships that could have appeared to influence the work reported in this paper.

Acknowledgments

This study was supported by the National Natural Science Foundation of China (No. 82272572, No. 82230085 and No. 81730068), the Science and Technology Major Project of Changsha (No. kh2102015), the Chinese Medicine Research Project of Fujian Province (2017FJZYLC305), and the Fundamental Research Funds for the Central Universities of Central South University (2022ZZTS0880).

Appendix A. Supplementary data

Supplementary data to this article can be found online at https://doi.org/10.1016/j.jot.2023.03.001.

References

[1] Rossetti L, Kuntz LA, Kunold E, Schock J, Müller KW, Grabmayr H, et al. The microstructure and micromechanics of the tendon-bone insertion. Nat Mater 2017;16(6):664–70 [eng].
[2] Genin GM, Thomopoulos S. The tendon-to-bone attachment: unification through disarray. Nat Mater 2017;16(6):607–8 [eng].
[3] Novakova SS, Mahalingam VD, Florida SE, Mendias CL, Allen A, Arruda EM, et al. Tissue-engineered tendon constructs for rotator cuff repair in sheep. J Orthop Res 2018;36(1):289–99 [eng].
[4] Zhao S, Su W, Shah V, Hobson D, Yildirimer L, Yeung KWK, et al. Biomaterials based strategies for rotator cuff repair. Colloids Surf B Biointerfaces 2017;157:407–16 [eng].
[5] Xu D, Zhang T, Qu J, Hu J, Lu H. Enhanced patella-patellar tendon healing using combined magnetic fields in a rabbit model. Am J Sports Med 2014;42(10):2495–501 [eng].
[6] Walsh WR, Harrison JA, Van Sickle D, Alvis M, Gillies RM. Patellar tendon-to-bone healing using high-density collagen bone anchor at 4 years in a sheep model. Am J Sports Med 2004;32(1):91–5 [eng].
[7] Galatz LM, Ball CM, Teefey SA, Middleton WD, Yamaguchi K. The outcome and repair integrity of completely arthroscopically repaired large and massive rotator cuff tears. J Bone Joint Surg Am 2004;86(2):219–24 [eng].
[8] Tang Y, Chen C, Liu F, Xie S, Qu J, Li M, et al. Structure and ingredient-based biomimetic scaffolds combining with autologous bone marrow-derived mesenchymal stem cell sheets for bone-tendon healing. Biomaterials 2020;241:119837 [eng].
[9] Tarafder S, Brito JA, Minhas S, Effiong L, Thomopoulos S, Lee CH. In situ tissue engineering of the tendon-to-bone interface by endogenous stem/progenitor cells. Biofabrication 2019;12(1):015008 [eng].
[10] Grässel SG. The role of peripheral nerve fibers and their neurotransmitters in cartilage and bone physiology and pathophysiology. Arthritis Res Ther 2014;16(6):485 [eng].
[11] Hu J, Qu J, Xu D, Zhang T, Qin L, Lu H. Combined application of low-intensity pulsed ultrasound and functional electrical stimulation accelerates bone-tendon junction healing in a rabbit model. J Orthop Res 2014;32(2):204–9 [eng].
[12] Zhang T, Chen Y, Chen C, Li S, Xiao H, Wang L, et al. Treadmill exercise facilitated rotator cuff healing is coupled with regulating periphery neuropeptides expression in a murine model. J Orthop Res 2021;39(3):680–92 [eng].
[13] Chen Y, Zhang T, Wan L, Wang Z, Li S, Hu J, et al. Early treadmill running delays rotator cuff healing via Neuropeptide Y mediated inactivation of the Wnt/β-catenin signaling. J Orthop Translat 2021;30:103–11 [eng].
[14] Ackermann PW, Franklin SL, Dean BJ, Carr AJ, Salo PT, Hart DA. Neuronal pathways in tendon healing and tendinopathy–update. Front Biosci (Landmark Ed) 2014;19(8):1251–78 [eng].
[15] Körner A, Schlegel M, Kaussen T, Gudernatsch V, Hansmann G, Schumacher T, et al. Sympathetic nervous system controls resolution of inflammation via regulation of repulsive guidance molecule A. Nat Commun 2019;10(1):633 [eng].
[16] Niedermair T, Kuhn V, Doranehgard F, Stange R, Wieskötter B, Beckmann J, et al. Absence of substance P and the sympathetic nervous system impact on bone structure and chondrocyte differentiation in an adult model of endochondral ossification. Matrix Biol 2014;38:22–35 [eng].
[17] Lorenz J, Schäfer N, Bauer R, Jenei-Lanzl Z, Springorum RH, Grässel S. Norepinephrine modulates osteoarthritic chondrocyte metabolism and inflammatory responses. Osteoarthritis Cartilage 2016;24(2):325–34 [eng].
[18] Zhang B, Ma S, Rachmin I, He M, Baral P, Choi S, et al. Hyperactivation of sympathetic nerves drives depletion of melanocyte stem cells. Nature 2020;577(7792):676–81 [eng].
[19] Lebaschi AH, Deng XH, Camp CL, Zong J, Cong GT, Carballo CB, et al. Biomechanical, histologic, and molecular evaluation of tendon healing in a new murine model of rotator cuff repair. Arthroscopy 2018;34(4):1173–83 [eng].
[20] Demas GE, Bartness TJ. Novel method for localized, functional sympathetic nervous system denervation of peripheral tissue using guanethidine. J Neurosci Methods 2001;112(1):21–8 [eng].
[21] Wang Z, Chen Y, Xiao H, Li S, Zhang T, Hu J, et al. The enhancement effect of acetylcholine and pyridostigmine on bone-tendon interface healing in a murine rotator cuff model. Am J Sports Med 2021;49(4):909–17 [eng].
[22] Bell R, Taub P, Cagle P, Flatow EL, Andarawis-Puri N. Development of a mouse model of supraspinatus tendon insertion site healing. J Orthop Res 2015;33(1):25–32 [eng].
[23] Wada S, Lebaschi AH, Nakagawa Y, Carballo CB, Uppstrom TJ, Cong GT, et al. Postoperative tendon loading with treadmill running delays tendon-to-bone healing: immunohistochemical evaluation in a murine rotator cuff repair model. J Orthop Res 2019;37(7):1628–37 [eng].
[24] Chen H, Wang Z, Zhou L, Wu B, Lu H, Zhang C, et al. Recombinant human bone morphogenetic protein-4 enhances tendon-to-bone attachment healing in a murine model of rotator cuff tear. Ann Transl Med 2021;9(7):565 [eng].
[25] Lu H, Chen C, Qu J, Chen H, Chen Y, Zheng C, et al. Initiation timing of low-intensity pulsed ultrasound stimulation for tendon-bone healing in a rabbit model. Am J Sports Med 2016;44(10):2706–15 [eng].
[26] Lu H, Liu F, Chen H, Chen C, Qu J, Xu D, et al. The effect of low-intensity pulsed ultrasound on bone-tendon junction healing: initiating after inflammation stage. J Orthop Res 2016;34(10):1697–706 [eng].
[27] Ackermann PW, Salo P, Hart DA. Tendon innervation. Adv Exp Med Biol 2016;920:35–51 [eng].
[28] Ackermann PW. Neuronal regulation of tendon homoeostasis. Int J Exp Pathol 2013;94(4):271–86 [eng].
[29] Long H, Ahmed M, Ackermann P, Stark A, Li J. Neuropeptide Y innervation during fracture healing and remodeling. A study of angulated tibial fractures in the rat. Acta Orthop 2010;81(5):639–46 [eng].
[30] Ivie TJ, Bray RC, Salo PT. Denervation impairs healing of the rabbit medial collateral ligament. J Orthop Res 2002;20(5):990–5 [eng].
[31] Ashrafi M, Baguneid M, Bayat A. The role of neuromediators and innervation in cutaneous wound healing. Acta Derm Venereol 2016;96(5):587–94 [eng].
[32] Schubert TE, Weidler C, Lerch K, Hofstädter F, Straub RH. Achilles tendinosis is associated with sprouting of substance P positive nerve fibres. Ann Rheum Dis 2005;64(7):1083–6 [eng].
[33] Ljung BO, Forsgren S, Fridén J. Substance P and calcitonin gene-related peptide expression at the extensor carpi radialis brevis muscle origin: implications for the etiology of tennis elbow. J Orthop Res 1999;17(4):554–9 [eng].
[34] Matheis F, Muller PA, Graves CL, Gabanyi I, Kerner ZJ, Costa-Borges D, et al. Adrenergic signaling in muscularis macrophages limits infection-induced neuronal loss. Cell 2020;180(1):64–78. e16. [eng].
[35] Pongratz G, Straub RH. The sympathetic nervous response in inflammation. Arthritis Res Ther 2014;16(6):504 [eng].
[36] Kunos G. Adrenoceptors. Annu Rev Pharmacol Toxicol 1978;18:291–311 [eng].
[37] Motyl KJ, Rosen CJ. The skeleton and the sympathetic nervous system: it's about time. J Clin Endocrinol Metab 2012;97(11):3908–11 [eng].
[38] Jenei-Lanzl Z, Grässel S, Pongratz G, Kees F, Miosge N, Angele P, et al. Norepinephrine inhibition of mesenchymal stem cell and chondrogenic progenitor cell chondrogenesis and acceleration of chondrogenic hypertrophy. Arthritis Rheumatol 2014;66(9):2472–81 [eng].
[39] Hedderich J, El Bagdadi K, Angele P, Grässel S, Meurer A, Straub RH, et al. Norepinephrine inhibits the proliferation of human bone marrow-derived mesenchymal stem cells via β2-adrenoceptor-mediated ERK1/2 and PKA phosphorylation. Int J Mol Sci 2020;21(11) [eng].
[40] Yirmiya R, Goshen I, Bajayo A, Kreisel T, Feldman S, Tam J, et al. Depression induces bone loss through stimulation of the sympathetic nervous system. Proc Natl Acad Sci U S A 2006;103(45):16876–81 [eng].
[41] Elefteriou F. Impact of the autonomic nervous system on the skeleton. Physiol Rev 2018;98(3):1083–112 [eng].
[42] Jiao K, Niu L, Xu X, Liu Y, Li X, Tay FR, et al. Norepinephrine regulates condylar bone loss via comorbid factors. J Dent Res 2015;94(6):813–20 [eng].
[43] Xu X, Li X, Liang Y, Ou Y, Huang J, Xiong J, et al. Estrogen modulates cartilage and subchondral bone remodeling in an ovariectomized rat model of postmenopausal osteoarthritis. Med Sci Mon Int Med J Exp Clin Res 2019;25:3146–53 [eng].